

Memories from the ergodic phase: the awkward dynamics of spherical mixed p -spin models

Giampaolo Folena,^{1,2} Silvio Franz,^{1,2} and Federico Ricci-Tersenghi^{1,3}

¹*Dipartimento di Fisica, Università “La Sapienza”, P.le A. Moro 5, 00185, Rome, Italy*

²*LPTMS, UMR 8626, CNRS, Univ. Paris-Sud, Université Paris-Saclay, 91405 Orsay, France*

³*INFN, Sezione di Roma1, and CNR–Nanotec, Rome unit, P.le A. Moro 5, 00185, Rome, Italy*

(Dated: May 16, 2022)

We revisit the long-time limit of the out of equilibrium dynamics of mean-field spherical mixed p -spin models. We consider quenches (gradient descent dynamics) starting from initial conditions thermalized at some temperature in the ergodic phase. We perform numerical integration of the dynamical mean-field equations of the model and we find an unexpected dynamical phase transition. Below an onset temperature T_{onset} , higher than the dynamical transition temperature T_{MCT} , the asymptotic energy goes below the “threshold energy” of the dominant marginal minima of the energy function and memory of the initial condition is kept. This behavior, not present in the pure spherical p -spin, resembles closely the one observed in simulations of glass forming liquids. We then investigate the nature of asymptotic dynamics, finding an aging state that relaxes towards deep marginal minima. Careful analysis however rules out simple aging solutions, leaving open a full comprehension of the memory effect in these models.

In the physics of glassy systems, the connection between dynamics and the underlying energy landscape is of crucial importance. A widely used characterization of the energy landscape sampled by the glassy dynamics is the numerical study of the inherent structures (ISs), defined as the local minima of the energy potential reached by a steepest descent [1, 2]. In simulations of glass forming liquids, it is observed that starting from thermalized configurations at temperature T , the energy of the corresponding ISs concentrates around a value $E_{\text{IS}}(T)$ that depends on T only below a characteristic onset temperature T_{onset} . Remarkably this temperature is higher than the estimated mode coupling critical temperature T_{MCT} .

According to the common belief, this temperature dependence should not appear in mean-field models: initial conditions thermalized above T_{MCT} would all have the same value of the IS energy and any memory of the initial condition (as well as of any configuration reached by the dynamics) would be lost after a long enough time. This belief is based on the solution of the spherical pure p -spin model [3] that has played a central role, because of two key features. Firstly, one can write closed equations for correlation and response functions [4] that can be solved analytically in the asymptotic regime of large times [5] and numerically for (large) finite times [6]. Secondly, the (free) energy landscape can be studied via thermodynamics and through the statistical analysis of the properties of stationary states [7, 8]. Remarkably a very precise connection between dynamics and landscape emerges. The model has an ideal mode-coupling dynamical transition at T_{MCT} , where ergodicity breaks and the dynamics fails to converge to equilibrium. Starting from any thermalized configuration at $T > T_{MCT}$, the zero-temperature dynamics converges to ISs whose energy E_{th} (the so-called threshold energy) is independent of T and can be evaluated via thermodynamic computations as the energy of the highest minima of the Hamiltonian.

However, the pure p -spin spherical model is rather

pathological. Its homogeneous Hamiltonian does not allow for state bifurcations or merging while changing the temperature, and this produces an energy landscape simpler than more generic mean-field models, like the Ising p -spin model, the Potts glass or even spherical models with mixtures of multi body interactions [9]. In the latter it has been realized that the computation of metastable states via standard replica calculation leads to puzzling results, with the disappearance of state-following solutions when the temperature becomes low enough [10].

In the present work we reexamine the off-equilibrium dynamics of the mixed p -spin spherical model, where the Hamiltonian is a random Gaussian function on the N -dimensional sphere ($\sum_i \sigma_i^2 = N$) with covariance

$$\overline{H[\sigma]H[\tau]} = Nf(q_{\sigma\tau}) \quad \text{and} \quad q_{\sigma\tau} = \frac{1}{N} \sum_{i=1}^N \sigma_i \tau_i. \quad (1)$$

$f(q)$ is a polynomial with positive coefficients chosen in a way that the model has a random first order (RFOT) or one step replica symmetry breaking (1RSB) transition. While the pure p -spin model corresponds to the case of a single monomial $f(q) = \frac{1}{2}q^p$, we study a larger and more generic class of polynomials f where at least two coefficients are positive (mixed p -spin model). All our numerical results are presented for $f(q) = \frac{1}{2}(q^3 + q^4)$, and compared with the pure case with $p = 3$.

To investigate how much of the above picture based on the solution of the pure p -spin model is generic and does apply to mixed p -spin models as well, we perform a high precision integration of the dynamical equations describing the evolution of the system in the thermodynamic limit, starting from a thermalized initial condition at temperature T and subsequently undergoing a gradient descent dynamics. Our main finding is that the above picture is not generic and inhomogeneous models show several unexpected features. The value of the asymptotic energy predicted under the assumption of aging with loss

of memory is only found starting from high enough temperatures. We find strong evidence for the existence of an onset temperature $T_{\text{onset}} > T_{\text{MCT}}$ below which the energy of the IS does depend of the initial temperature T and goes below the threshold value.

Out-of-equilibrium equations Given the Hamiltonian (1), we consider the Langevin dynamics:

$$\begin{aligned} \partial_t \sigma_i(t) &= -\mu(t)\sigma_i(t) - \frac{\partial H}{\partial \sigma_i}(t) + \xi_i(t) \quad (2) \\ \langle \xi_i(t)\xi_j(t') \rangle &= 2T_f \delta_{ij} \delta(t-t') \\ P[\sigma(0)] &= \frac{e^{-\beta H(\sigma(0))}}{Z(\beta)} \end{aligned}$$

where T_f is the temperature of the thermal bath (later

set to zero) and $\beta = 1/T$ is the inverse temperature at which the initial condition is equilibrated. $\mu(t)$ is the Lagrange multiplier that constrains the dynamics on the sphere, and for any time t it takes the value

$$\mu(t) = T_f - \frac{1}{N} \sum_i \sigma_i(t) \frac{\partial H}{\partial \sigma_i}(t), \quad (3)$$

that we call radial reaction force.

In the thermodynamic limit $N \rightarrow \infty$ and finite times, the equations (2) imply closed integro-differential equations [4, 11, 12] for the correlation $C(t, t') \equiv \langle \sigma_i(t)\sigma_i(t') \rangle$ and for the response $R(t, t') \equiv \frac{\partial \langle \sigma_i(t) \rangle}{\partial \xi_i(t')}$, that for an initial temperatures T greater than the Kauzmann temperature of thermodynamic phase transition T_K read [13]:

$$\begin{aligned} \partial_t C(t, t') &= -\mu(t)C(t, t') + \int_0^t ds f''(C(t, s))R(t, s)C(s, t') + \int_0^{t'} ds f'(C(t, s))R(t', s) + \beta f'(C(t, 0))C(t', 0) \\ \partial_t R(t, t') &= -\mu(t)R(t, t') + \int_{t'}^t ds f''(C(t, s))R(t, s)R(s, t') \quad (4) \\ \mu(t) &= T_f + \int_0^t ds f''(C(t, s))R(t, s)C(t, s) + \int_0^t ds f'(C(t, s))R(t, s) + \beta f'(C(t, 0))C(t, 0) \end{aligned}$$

The energy of the system at time t is expressed in terms of $C(t, t')$ and $R(t, t')$ as

$$E(t) = - \int_0^t f'(C(t, s))R(t, s)ds - \beta f(C(t, 0)) \quad (5)$$

The initial condition enters the above equations in a rather simple way, and for $\beta = 0$ the equations reduce to the usual form valid for white initial condition.

These equations have a causal structure, and can be integrated numerically by time discretization. The simplest possibility, which we adopt here, is a fixed time-step Δt first-order Euler algorithm, that gives very reliable results at short time [14]. Other algorithms with variable time step have been proposed and used in the literature [6, 15]. Unfortunately in our case, as soon as $\beta > 0$ and we consider a p -spin mixture, these algorithms appear to be unstable at short times and do not allow any improvements over the simple one. With such a simple integration scheme and a maximum step of $\Delta t = 0.1$, we reach times of order 10^3 . On these time scales, the dynamics is in most interesting cases quite far from its asymptotic behavior and an estimate of the large time energy would not be reliable. For that reason we limit ourself in this paper to zero temperature dynamics, where energy monotonically decreases and once below threshold it cannot bounce up again.

Affinities and divergences between mixed and pure models We enter here into the core question of this Letter, and compare the energy reached by the dynamics from different initial conditions, to the threshold energy

that can be computed from the asymptotic solution with $\beta = 0$ [5] or by computation of the complexity of minima [16]. For the 3+4 model the value of the threshold energy is $E_{th} = -71/42 \simeq -1.6905$. In Fig. 1 we show the curves of the energy as a function of time for different T , ranging from $T = \infty$ to $T = 0.796$, the dynamical transition temperature of the model being $T_{\text{MCT}} = 0.805$. Data are obtained from an integration with step $\Delta t = 0.1$, reaching the maximum time of 2500. This step size gives a relative integration error smaller than 10^{-5} (see SM).

On the time scale we can reach, and temperatures $T \gtrsim 1$ the energy as a function of time seems to have reached an asymptotic behavior and the lines are very well fitted by a power law $E(t) = E_{th} + a/t^\gamma$ with a slightly dependent on temperature and $\gamma = 0.64 \pm 0.01$, making us confident that E_{th} is the asymptotic value of the energy in this range of temperatures. On the other hand, if T is small enough but still larger than T_{MCT} , the curves of the energy go below E_{th} . For comparison in the upper inset we present the same curves for the pure model with $p = 3$. In that case manifestly the energy tends to the threshold value for all $T \geq T_{\text{MCT}}$. These results suggest a scenario with a new dynamical transition in the mixed model, with an onset temperature T_{onset} separating a memoryless phase for $T > T_{\text{onset}}$ from phase at $T < T_{\text{onset}}$ that keeps some memory of the initial condition. It is also interesting to look at $T < T_{\text{MCT}}$. In our data we do not observe anything special happening at T_{MCT} , it is only below a temperature $T_{\text{SF}} \approx 0.798$ that we observe relaxation becoming fast and the energy decay-

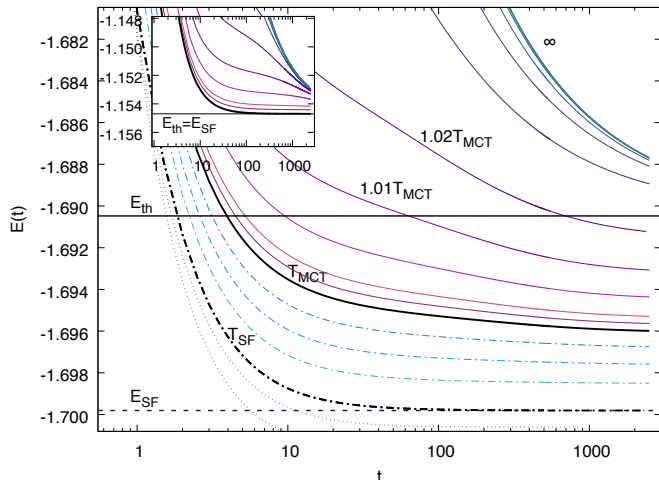


FIG. 1. Energy relaxation in the (3+4)-spin model, starting from different temperatures T and quenching to zero temperature. Continuous lines are quenches from the ergodic phase ($T \geq T_{\text{MCT}} = 0.805$), from bottom to top $T/T_{\text{MCT}} = 1, 1.001, 1.002, 1.005, 1.01, 1.02, 1.05, 1.1, 1.2, 1.5, 2, 4, 10, \infty$. The dashed-dotted lines correspond to quenches from $T_{\text{SF}} = 0.9914T_{\text{MCT}} = 0.798 \leq T < T_{\text{MCT}}$, from top to bottom $T/T_{\text{MCT}} = 0.998, 0.996, 0.994, 0.992$ and a last at T_{SF} . The dotted lines correspond to $T < T_{\text{SF}}$, $T/T_{\text{MCT}} = 0.99, 0.988$. We clearly see that the energy goes below threshold for temperatures that are small enough, although larger than T_{MCT} . Inset: same dynamics for the 3-spin model ($T \geq T_{\text{MCT}}$), the energy never goes below threshold.

ing exponentially to its asymptote. We will see that we can predict the asymptotic energy in this region through a quasi-static solution of the dynamical equations ('state following' with memory of the initial condition).

We remark that a small temperature T_f in the dynamical equations does not change this behavior. Also in that case we observe the energy to go below the asymptotic value valid for white initial conditions. In that case however, although very unlikely, we cannot completely exclude the possibility that after an initial decrease the energy would go up again to its memoryless limit. In that case, contrary to common sense expectation, one would obtain $E_{th} = \lim_{T_f \rightarrow 0} \lim_{t \rightarrow \infty} E(t) > \lim_{t \rightarrow \infty} \lim_{T_f \rightarrow 0} E(t)$.

In order to understand the dynamical mechanisms that allow to beat the threshold, we look at the behavior of response and correlations. A first quantity we would like to understand is the correlation with the initial state, $C(t, 0)$. According to the usual weak ergodicity breaking scenario this quantity should vanish at large t . Both in the mixed and in the pure model we observe that the relaxation of $C(t, 0)$ is slower and slower as T decreases. As for the energy we can identify three temperature regimes for $T > T_K$: (I) a high temperature regime $T > T_{\text{onset}}$ where memory of the initial condition is lost and $C(t, 0) \rightarrow 0$; (II) an intermediate 'hic sunt leones'

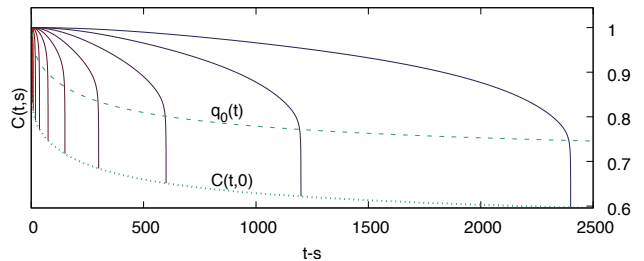


FIG. 2. Correlation function $C(t, s)$ at $T = 0.813 = 1.01T_{\text{MCT}}$ as a function of $t - s$ for fixed values of $t = 2400 \cdot 2^{-n}$ with $n = 0, \dots, 9$ (from right to left). The correlation shows clear aging features, becoming slower for larger times. After the slow decay, at a well defined value $q_0(t)$ (dashed line), the correlation display a sudden drop to $C(t, 0)$ (dotted line).

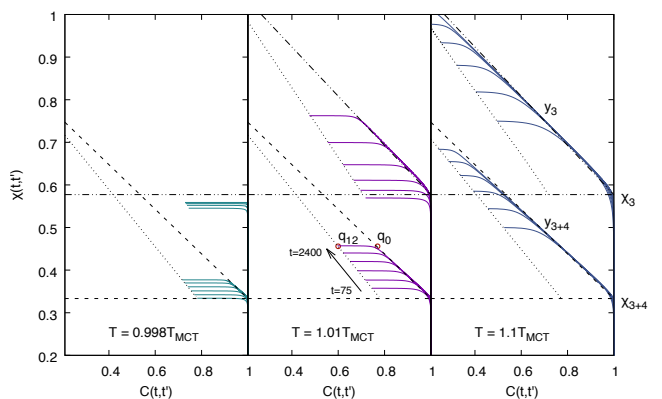


FIG. 3. Integrated response $\chi(t, t')$ versus correlation $C(t, t')$ for three different temperatures $T/T_{\text{MCT}} = 0.998, 1.01, 1.1$. The lines are plotted fixing $t = 75, 150, 300, 600, 1200, 2400$ (from bottom to top) and changing t' . In all the panels upper data are for the 3-spin model and lower data for the (3+4)-spin model. The dashed/dotted lines indicate the susceptibility χ_{th} and the fluctuation dissipation ratio y_0 predicted by the memoryless solution. It interesting to note that in the (3+4)-spin model the dynamics does not have any appreciable change at T_{MCT} , while in the 3-spin model, starting below T_{MCT} , the system remains trapped in a state.

regime $T_{\text{SF}} < T < T_{\text{onset}}$ where the relaxation is slow and any extrapolation is difficult; (III) a low temperature regime $T < T_{\text{SF}}$ where $C(t, 0)$ relaxes exponentially fast to a non zero value q_{12} .

While no aging is found in regime III, in regimes I and II we find aging, qualitatively similar in the two cases. In Fig. 2 we show $C(t, s)$ as a function of $t - s$ for several times t at temperature $T = 1.01T_{\text{MCT}}$. The curves show a clear aging behavior with the dynamics decorrelating slower and slower as time passes, followed by a fast drop of the correlation for small values of s to the value $C(t, 0)$.

Aging behavior is often qualified studying the effective temperature emerging from the relation between response and correlation [17]. Fig. 3 shows the parametric

plot of the integrated response $\chi(t, s) \equiv \int_s^t R(t, u) du$ versus $C(t, s)$ as a function of s for various values of t . In zero temperature dynamics the integrated response has a jump in $C = 1$ to χ_{EA} . The asymptotic weak ergodicity breaking solution [5] predicts $\chi_{EA} = \chi_{th} \equiv 1/\sqrt{f''(1)}$ and a linear behavior for $C < 1$ with slope given by the ‘fluctuation-dissipation ratio’ $y_0 \equiv \sqrt{f''(1)}/f'(1) - \chi_{th}$. The relation $\chi_{EA} = \chi_{th}$ is true in any solution assuming asymptotic convergence towards marginal states.

On the time scales we can access, both the pure and the mixed models show, for all the values of $T > T_{SF}$, a jump and a linear part in agreement with the memoryless solution [18]. This holds till a well defined time dependent value of the correlation $q_0(t) > C(t, 0)$ where the response essentially stops to increase. $q_0(t)$ identified in Fig. 2 marks the value that separates slow dynamics, where an effective temperature emerges, from fast partial decorrelation from the initial condition, during which the system does not respond. The extrapolation of $q_0(t)$ at large time presents the same difficulties as that of $C(t, 0)$.

Further evidence that the dynamics is relaxing towards marginal states is provided by the radial reaction $\mu(t)$ that clearly converges to the marginal value $\mu_{th} \equiv 2\sqrt{f''(1)}$ for any $T > T_{SF}$ (data is shown in the SM). In the pure model $\mu = pE$ holds and thus $\mu(t) \rightarrow \mu_{th} \implies e(t) \rightarrow e_{th}$, while in the mixed model marginal states ($\mu = \mu_{th}$) may have different energies.

Ansätze for asymptotic solutions The dependence of the final energy on T in regime II testifies a form of memory of the initial condition. Differently thermalized configurations lie in basins of attraction of different marginal states. The asymptotic ansatz of Cugliandolo and Kurchan has been generalized in [9] supposing ‘aging within a metabasin’ and a non vanishing correlation with the initial state $\lim_{t \rightarrow \infty} C(t, 0) = q_{12} > 0$. Unfortunately, the resulting equations for χ, y, q_{12}, q_0 only have an aging solution different from the ‘amnesic’ one ($q_{12} = q_0 = 0$) in the interval $T_{SF} \leq T \leq T_0 = 0.803 < T_{MCT}$. Even when the solution exists, the values of the various parameters do not match the observations, in particular one finds $y \approx 0.3$ while in dynamics $y \approx 0.52$. This aging solution terminates at the temperature T_{SF} where q_0 tends to one. Below that temperature, there is a stable ‘state following’ solution with no aging, $q_{12} > 0$, $\mu > \mu_{th}$ and $\chi < \chi_{th}$ (see SM). This solution correctly reproduces the asymptotic values of the energy, correlation, radial reaction of the large time dynamics for temperatures $T \lesssim T_{SF}$.

Despite all efforts, we have been unable to find a different asymptotic dynamical ansatz describing aging in the ‘hic sunt leones’ regime II and/or to find in the numerics an indication on where the memory of the initial condition could affect the asymptotic solution. Insisting in using a 1RSB dynamical ansatz with $\chi_{EA} = \chi_{th}$, $\mu = \mu_{th}$ and $y = y_0$, which is supported by the numerical solution, one can easily derive the following relation

$$y_0 f'(q_0) q_0 = \beta f'(q_{12}) q_{12}. \quad (6)$$

A second relation can be obtained from the observation

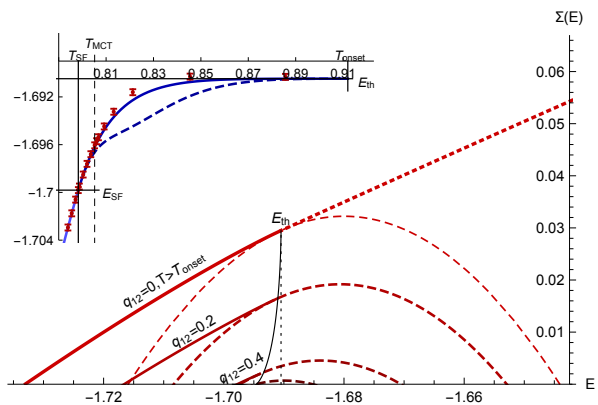


FIG. 4. Quenched constrained complexity $\Sigma(E, \mu, q_{12}, T)$ in the (3+4)-spin model. The upper full line is the complexity of the dominant stable minima ($q_{12} = 0$). Its dashed continuation above E_{th} represents dominant saddles. The dashed parabola underneath is the complexity of marginal states ($\mu = \mu_{th}$). The same pattern is repeated for different couples $q_{12}, T(q_{12})$ with $q_{12} = 0.2, 0.4, 0.6$. Inset: numerically extrapolated asymptotic energy (data with errors), approximated asymptotic solution of dynamical equations (full line) and E_{th} from quenched constrained complexity (dashed line).

that $\chi_{tot}(t) \equiv \int_0^t ds R(t, s) \approx \chi_{th} + y_0(1 - q_0(t))$ depends linearly on $C(t, 0)$ even at finite times (see dotted lines in Fig. 3). Moreover this linear relation does not present any temperature dependence in the range $T_{SF} \leq T \lesssim 1$ (data shown in the SM) and implies a linear relation between q_{12} and q_0 that can be estimated from two analytically known limits: for T large enough $q_{12} = q_0 = 0$, while at $T = T_{SF}$ we have $q_0 = 1$ and $q_{12, SF} = \sqrt{1 - f'(1)/f''(1)}$ (see SM for details). Using the relation $q_{12} = q_{12, SF} q_0$, Eq. (6) admits a solution with $q_{12}, q_0 > 0$ only if

$$T < T_{onset} \equiv \frac{q_{12, SF}^k}{y_0} = \frac{f'(1)[f''(1) - f'(1)]^{\frac{k}{2}-1}}{f''(1)^{\frac{k-1}{2}}}, \quad (7)$$

where k is defined by $f(q) \propto q^k$ for $q \rightarrow 0$ (in the 3+4-model $T_{onset} = 0.91$). Despite this is not an exact solution of the asymptotic equations, it is a strong indication that the passage from memoryless to memorious aging is marked by a phase transition.

Counting energy minima In the attempt to connect the asymptotic dynamics to the energy landscape we studied the energy minima which are possible attractors for the gradient descent dynamics. We count the stationary points of the Hamiltonian $H[\sigma]$ on the sphere $\sum_i \sigma_i^2 = N$ with energy $E = \frac{1}{N} H[\sigma]$, radial reaction $\mu = \sum_i \sigma_i H'_i / N$ and overlap q_{12} with respect to an equilibrium configuration at temperature T . It is well known [19, 20] that the spectrum of the Hessian in the stationary points of these models is a shifted Wigner semicircle law. Its support is strictly positive only if $\mu > \mu_{th}$. All and only the marginal minima have $\mu = \mu_{th}$ and $\chi = \chi_{th}$, which are the attractors of dynamics for $T > T_{SF}$. In Fig. 4 we show for the (3+4)-model the

total ($q_{12} = 0$) and constrained ($q_{12} > 0$) quenched complexity $\Sigma(E, \mu, q_{12}, T)$ [21] (mean logarithm of number of stationary points): when $q_{12} > 0$ we fix $T = T(q_{12}) \equiv f'(q_{12})q_{12}/[y_0 f'(q_{12}/q_{12, \text{SF}})q_{12}/q_{12, \text{SF}}]$ via Eq. (6). At variance to pure models, where $\mu = pE$, we see that marginal states ($\mu = \mu_{th}$) exist in a broad range of energies (dashed parabolas). The most numerous states at each energy are shown with full lines (minima) or dotted lines (saddles). The energy $E_{th}(q_{12})$ of the endpoint of the continuous line is the best candidate to describe the long time dynamics when $\lim_{t \rightarrow \infty} C(t, 0) = q_{12}$ (indeed $E_{th}(0) = E_{th}$). The complexity gives a qualitatively correct explanation: increasing q_{12} the largest energy where marginal states dominates decreases, as seen in the numerical integration. However, a more quantitative comparison (see the inset of Fig. 4) suggests that the commonly accepted connection between dominating marginal states (dashed curve) and long time aging dynamics (datapoint with errors) fails in the ‘hic sunt leones’ region $T_{\text{SF}} < T < T_{\text{onset}}$, while the approximate asymptotic solution is much more accurate (full line).

Conclusions We have studied the zero temperature relaxation dynamics of spherical mixed p -spin models, initially thermalized at temperature T . We have found a temperature region $T_{\text{SF}} < T < T_{\text{onset}}$ where the asymptotic dynamics, although marginal, does depend on T and keeps memory of finite times. This resembles realistic glass former, but was unexpected in mean field models. We have found an approximate description for the asymptotic dynamics that provides, for the first time, an

analytic prediction for the onset temperature. The exact solution to the asymptotic dynamics is still unknown.

We have computed the quenched complexity constrained to a given overlap q_{12} with respect to an equilibrium configuration at temperature T and consequently defined the marginal threshold states. However these states do not have the same properties measured in the asymptotic dynamics. So the connection between asymptotic dynamics and energy landscape is still very open in spherical mixed p -spin models.

Pure p -spin models have strong symmetries leading to $T_{\text{SF}} = T_{\text{onset}} = T_{\text{MCT}}$: so they lack some realistic features of glass formers (e.g. onset temperature, chaos in temperature, Gardner transition) and has misled us for two decades with a too simplistic connection between dynamics and energy landscape. Mixed models appear to be much better models than pure ones to describe the dynamical onset of glassy phenomenology, they have much more complex energy landscapes, which deserve to be better studied in the future. Research is needed in two directions: one should find algorithms capable of reaching large times in solving the dynamical equations and new theoretical ideas on possible structures of the memory aging are necessary to understand the asymptotic aging regime.

We thank Giorgio Parisi for several important discussions. This research has been supported by the Simons Foundation (grants No. 454941, S. Franz; No. 454949, G. Parisi) and by the European Research Council (ERC) under the European Unions Horizon 2020 research and innovation programme (grant No. 694925, G. Parisi).

-
- [1] S. Sastry, P. G. Debenedetti, and F. H. Stillinger, *Nature* **393**, 554 (1998).
- [2] F. Sciortino, W. Kob, and P. Tartaglia, *Physical Review Letters* **83**, 3214 (1999), arXiv: cond-mat/9906081.
- [3] A. Crisanti and H.-J. Sommers, *Zeitschrift für Physik B Condensed Matter* **87**, 341 (1992).
- [4] A. Crisanti, H. Horner, and H.-J. Sommers, *Zeitschrift für Physik B Condensed Matter* **92**, 257 (1993).
- [5] L. F. Cugliandolo and J. Kurchan, *Physical Review Letters* **71**, 173 (1993), arXiv: cond-mat/9303036.
- [6] B. Kim and A. Latz, *Europhysics Letters (EPL)* **53**, 660 (2001), arXiv: cond-mat/0005172.
- [7] J. Kurchan, G. Parisi, and M. Virasoro, *Journal de Physique I* **3**, 1819 (1993).
- [8] S. Franz and G. Parisi, *Journal de Physique I* **5**, 1401 (1995), arXiv: cond-mat/9503167.
- [9] A. Barrat, S. Franz, and G. Parisi, *Journal of Physics A: Mathematical and General* **30**, 5593 (1997), arXiv: cond-mat/9703091.
- [10] Y. Sun, A. Crisanti, F. Krzakala, L. Leuzzi, and L. Zdeborová, *Journal of Statistical Mechanics: Theory and Experiment* **2012**, P07002 (2012), arXiv: 1204.3734.
- [11] H. Sompolinsky and A. Zippelius, *Physical Review B* **25**, 6860 (1982).
- [12] M. Mezard, G. Parisi, and M. Virasoro, *Spin Glass Theory and Beyond: An Introduction to the Replica Method and Its Applications*, World Scientific Lecture Notes in Physics (World Scientific, 1987).
- [13] A. Barrat, R. Burioni, and M. Zzard, *Journal of Physics A: Mathematical and General* **29**, L81 (1996), arXiv: cond-mat/9511089.
- [14] S. Franz and M. Mezard, *Physica A: Statistical Mechanics and its Applications* **210**, 48 (1994), arXiv: cond-mat/9403004.
- [15] L. Berthier, G. Biroli, J.-P. Bouchaud, W. Kob, K. Miyazaki, and D. Reichman, *The Journal of Chemical Physics* **126**, 184504 (2007), arXiv: cond-mat/0609658.
- [16] A. Crisanti and H.-J. Sommers, *Journal de Physique I* **5**, 805 (1995).
- [17] L. F. Cugliandolo, J. Kurchan, and L. Peliti, *Physical Review E* **55**, 3898 (1997), arXiv: cond-mat/9611044.
- [18] Relative variations of χ and y comparable to the one we find in the energy cannot be excluded.
- [19] A. Cavagna, I. Giardina, and G. Parisi, *Physical Review B* **57**, 11251 (1998), arXiv: cond-mat/9710272.
- [20] A. Auffinger, G. B. Arous, and J. Cerny, arXiv:1003.1129 [math-ph] (2010), arXiv: 1003.1129.
- [21] B. Capone, T. Castellani, I. Giardina, and F. Ricci-Tersenghi, *Physical Review B* **74** (2006), 10.1103/PhysRevB.74.144301, arXiv: cond-mat/0603759.
- [22] G. B. Arous, E. Subag, and O. Zeitouni, arXiv:1804.10573 [math] (2018), arXiv: 1804.10573.

Supplementary Material for the manuscript
“Memories from the ergodic phase:
the awkward dynamics of spherical mixed p -spin models”

Giampaolo Folena, Silvio Franz and Federico Ricci-Tersenghi

I. NUMERICAL EXTRAPOLATIONS

The dynamical equations for the correlation and the response functions — Eq. (4) in the main text — were integrated via a simple Euler algorithm with a fixed integration step Δt . In this way we get extremely precise results at finite time, but the times we can reach are limited. We tried more sophisticated integration schemes [6], where the integration steps is increased during the evolution but unfortunately, as soon as a mixture is used we have met numerical instabilities at very short times. In practice only the pure p -spin model seems to allow those integration schemes to work.

The results presented in the main text have been obtained integrating with an optimal integration step $\Delta t = 0.1$, which allows us to reach the largest times without facing any numerical instability (consider that at short times the differential equations we are solving have a natural times scale of order 1, and so Δt cannot be much larger than the value we used).

The integration error in the Euler algorithm is linear in the integration step Δt , and we are interested in understanding how much physical quantities computed with $\Delta t = 0.1$ do differ from the corresponding $\Delta t \rightarrow 0$ limit. To this purpose we study the relative errors in one-time quantities defined as follows

$$\Delta_r x(t) = \frac{x(t; \Delta t) - x(t; \Delta t = 0.1)}{x(t; \Delta t)}. \quad (8)$$

By definition this relative error is zero for $\Delta t = 0.1$, should be linear in Δt for Δt small enough and in the limit $\Delta t \rightarrow 0$ provides the relative error committed in using an integration step $\Delta t = 0.1$ instead of the exact integration ($\Delta t \rightarrow 0$).

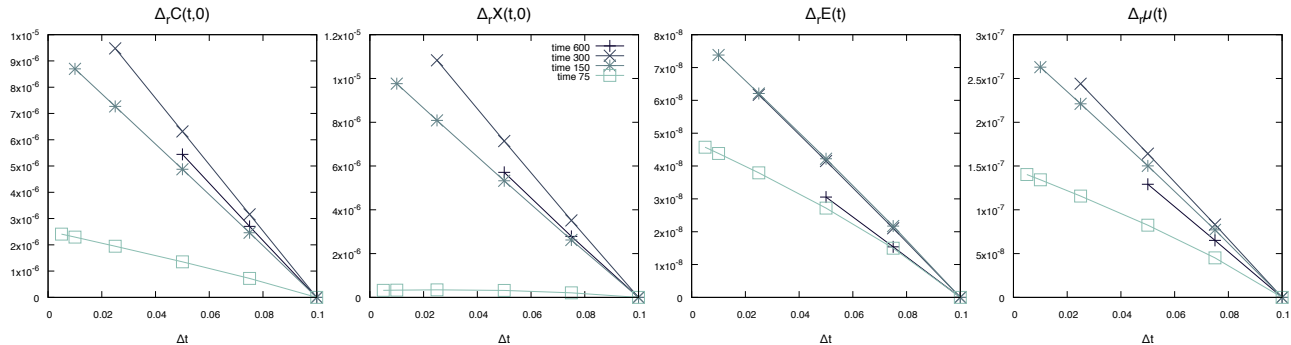


FIG. 5. The relative errors, as defined in Eq. (8), for $C(t, 0)$, $\chi(t, 0)$, $E(t)$ and $\mu(t)$ obtained in the integration of the dynamical equations for the (3+4)-spin with $T = T_{\text{MCT}}$. The dependence is linear in the integration step Δt and the resulting integration error in using $\Delta t = 0.1$ is very small compared to the precision needed in the asymptotic evaluation of the observables.

In Fig. 5 we show the relative errors in some one-time quantities, $C(t, 0)$, $\chi(t, 0)$, $E(t)$ and $\mu(t)$, obtained in the integration of the dynamical equations for the (3+4)-spin with $T = T_{\text{MCT}}$. We clearly see that at any time t the relative error scales roughly linear with Δt (higher order terms are visible only for the shortest time, $t = 75$). For any time t the relative errors are extremely small: of order 10^{-5} for correlation and response, and of order 10^{-7} for energy and radial reaction. Moreover the coefficient of the linear relation does not seem to grow with time, but actually show a maximum around $t \approx 300$. This is probably related to another important observation: trajectories integrated with different Δt may differ sensibly at short times, but at large times they seem to converge to the same asymptotic solution, which thus very attractive and stable (this may be the reason why integration errors at very large times are smaller than those at intermediate times). The results of the integration show in the present work are very reliable and stable. The numerical data can be easily extrapolated to $\Delta t \rightarrow 0$ by comparing different Δt , however, given the small error, this is not necessary given the precision we need.

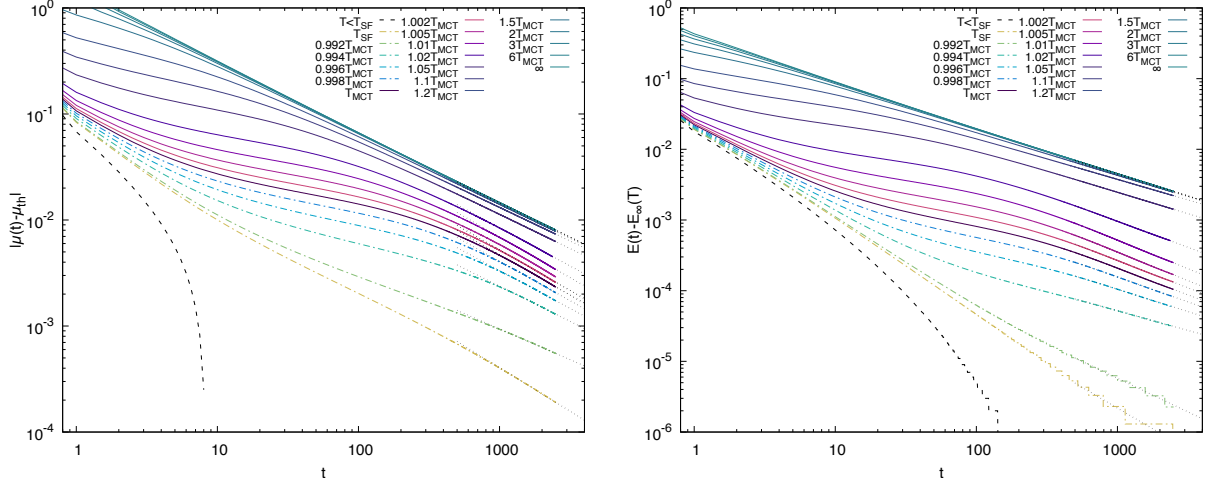


FIG. 6. Left: Decay of the radial reaction with time in the (3+4)-spin model on a double logarithmic scale. Its asymptotic value has been assumed equal to $\mu_{th} = 6$, which we believe to hold for $T \geq T_{SF}$. Right: Decay of the energy with time in the (3+4)-spin model on a double logarithmic scale. The asymptotic value $E_{\infty}(T)$ has been estimated as explain below via power law fits, that provide a good description of the asymptotic decay for $T \geq T_{SF}$.

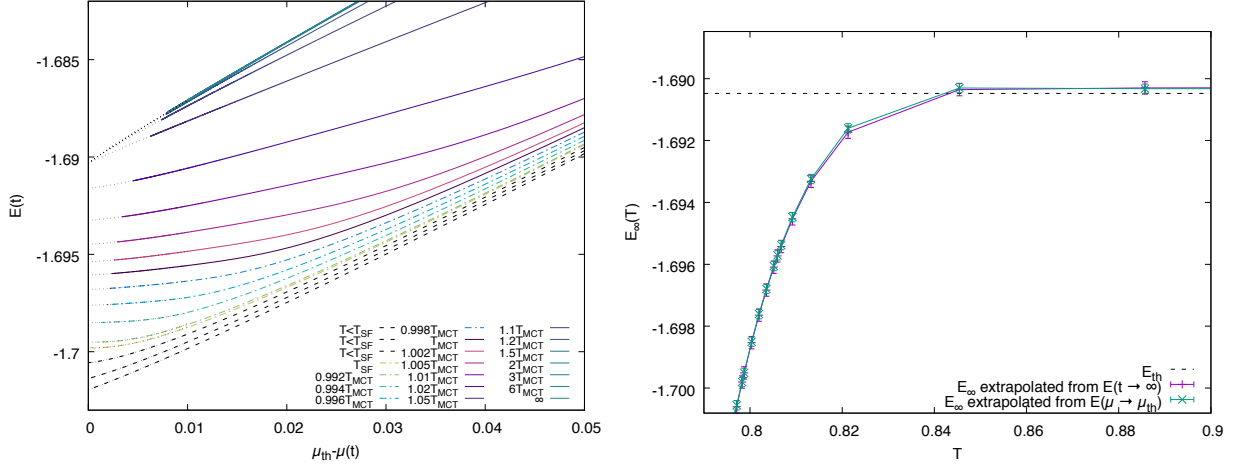


FIG. 7. Left: Parametric plot of $E(t)$ versus $\mu_{th} - \mu(t)$ varying t . The dotted lines are the best power law fits in the form $E = E_{\infty}(T) + A(T)(\mu_{th} - \mu)^{\alpha(T)}$ used to estimate the asymptotic energies. Right: Comparison of two different extrapolations of the asymptotic energies $E_{\infty}(T)$, obtained fitting versus t and versus $\mu_{th} - \mu(t)$.

Despite the high precision at finite times, the extrapolation to large t of physical quantities, notably $\mu(t)$, $E(t)$ or $C(t, 0)$ is delicate. While $C(t, 0)$ decays very slow and we do not attempt any extrapolation in the $t \rightarrow \infty$ limit, both $\mu(t)$ and $E(t)$ appear converge fast enough and their large time limits can be estimated.

First of all we notice that for $T \geq T_{SF}$ the radial reaction $\mu(t)$ is perfectly compatible with an extrapolation to the marginal value μ_{th} , where $\mu_{th} = 6$ in the (3+4)-spin model. To provide support to the this observation we show in the left plot of Fig. 6 data for $\mu(t) - \mu_{th}$ versus t in a double logarithmic. At very high temperatures the decay is pretty linear (i.e. a simple power law decay describes perfectly the data), while at lower temperatures we observe a pre-asymptotic relaxation, that eventually crosses over to the asymptotic decay. The latter seems to be characterized by an exponent which is roughly temperature independent.

Given critical character of the dynamics in the aging regimes I and II, we have estimated the asymptotic energy $E_{\infty}(T)$ via power law fits to $E(t)$ data and we show in the right panel of Fig. 6 the results. While at high temperatures the data follow a nice power law for about a couple of decades, at lower temperatures the presence of the pre-asymptotic regime and the crossover to the asymptotic one, makes very hard to assess the reliability of the value of $E_{\infty}(T)$ that we extrapolate in this way.

Comparing the data shown in the two panels of Fig. 6 for $\mu(t)$ and $E(t)$ we notice a very similar behavior (including the crossover) and thus it could be useful to plot parametrically $E(t)$ versus $\mu(t)$ varying t , and see whether a better estimation of $E_\infty(T)$ could be obtained. This is done in the left panel of Fig. 7. The behavior of the energy as a function of the radial reaction is very smooth, practically linear at high temperatures and close to quadratic approaching T_{SF} . We can then fit the relation $E(\mu)$ and obtain a good estimate of $E_\infty(T)$ just assuming that $\mu(t)$ converges to the marginal value μ_{th} in the large time limit. We have interpolated the data via the function

$$E(\mu) = E_\infty + A(\mu_{th} - \mu)^\alpha \quad (9)$$

and we report with dotted curves in the left panel of Fig. 6 the best fitting functions.

In the right plot of Fig. 6 we show the two estimates of $E_\infty(T)$ obtained from the procedures just described: the power law fit of energy versus time and the power law fit of energy versus radial reaction $\mu_{th} - \mu(t)$. We see they are perfectly compatible. The values for the extrapolated energy $E_\infty(T)$ are those reported in the inset of Fig. 4 in the main article.

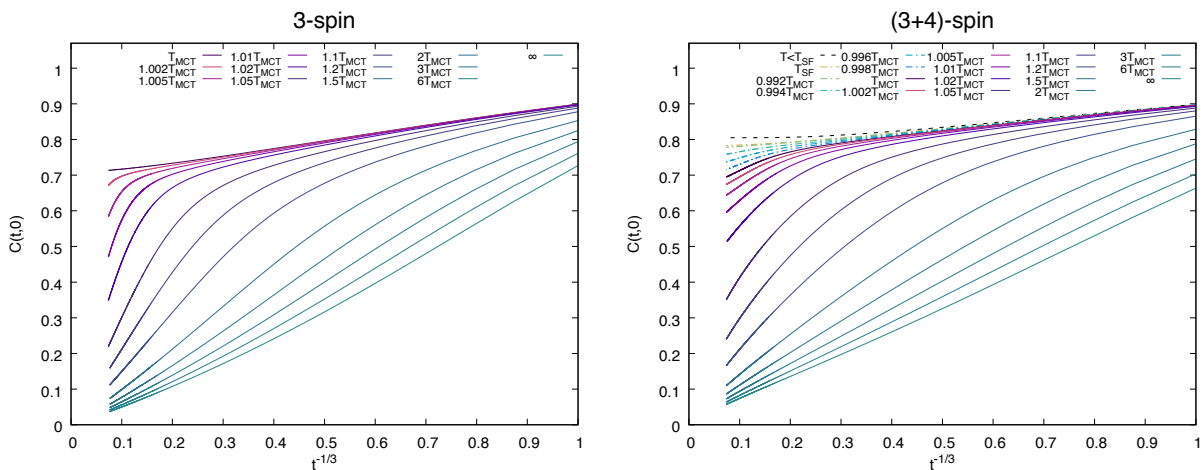


FIG. 8. Decay of the correlation with the initial configuration $C(t,0)$ vs $t^{-1/3}$ in the 3-spin model (left panel) and the (3+4)-spin model (right panel). Our choice for the x axis, $t^{-1/3}$, has been dictated by the request of making the relaxation from $T = \infty$ as linear as possible (notice however that the exact value for the decay exponent of $C(t,0)$ is unknown even in this case). While data for the 3-spin model can be easily extrapolated to zero in the large times limit, the data for the (3+4)-spin model seems much more compatible with a non-zero limit $\lim_{t \rightarrow \infty} C(t,0)$ when the temperature gets close to T_{MCT} .

Although we do not want to estimate the large time limit of $C(t,0)$ directly extrapolating in time (in Section III an estimate will be provided based on a different approach), we believe it is useful to show the $C(t,0)$ curves such that the reader can make her own idea. In Fig. 8 the data for $C(t,0)$ is shown, measured both in the pure 3-spin model and in the mixed (3+4)-spin model. We have decided to show these data as a function of the scaling variable $t^{-1/3}$ that describes pretty well the decay starting from a random configuration ($T = \infty$). En passant, we notice that the exact value for this decay is not known. We see in Fig. 8 that, while data for the 3-spin model can be easily extrapolated to zero in the large times limit, the data for the (3+4)-spin model seems much more compatible with a non-zero limit $\lim_{t \rightarrow \infty} C(t,0)$ when the temperature gets close to T_{MCT} .

II. ASYMPTOTIC SOLUTIONS

In Ref. [9] it was shown that the asymptotic solution to the dynamical equations assuming a simple memorious aging within a state with a unique effective temperature has parameters χ , q_0 , q_{12} and y that satisfy the same equations that can be obtained extremizing the Franz-Parisi (FP) potential computed in the one step replica symmetry breaking (1RSB) scenario, provided that the parameter y , is fixed by a marginality condition.

In our case the 1RSB FP potential has to be computed at zero temperature ($T_f = 0$), while the reference configuration is in equilibrium at temperature $T = 1/\beta$

$$-2V_{\text{1RSB}}(q_{12}, \chi, q_0, y) = \chi f'(1) + y(f(1) - f(q_0)) + \frac{1}{y} \log \left(\frac{\chi + y(1 - q_0)}{\chi} \right) + \frac{q_0 - q_{12}^2}{\chi + y(1 - q_0)} + 2\beta f(q_{12}). \quad (10)$$

The saddle point equations and the marginality condition thus read

$$\begin{cases} \partial_\chi V_{\text{IRSB}} = 0 & \implies \chi(1 - q_{12}^2) + y(1 - q_0)^2 - \chi(\chi + y(1 - q_0))^2 f'(1) = 0 \\ \partial_{q_0} V_{\text{IRSB}} = 0 & \implies q_0 - q_{12}^2 - (\chi + y(1 - q_0))^2 f'(q_0) = 0 \\ \partial_{q_{12}} V_{\text{IRSB}} = 0 & \implies q_{12} - \beta(\chi + y(1 - q_0))f'(q_{12}) = 0 \\ \text{marginality} & \implies \chi^2 f''(1) = 1 \end{cases} \quad (11)$$

We notice *en passant* that equations in (11) do not always select minima of the FP potential, because for that one needs to set to zero the total derivative with respect to q_{12} and not the partial derivative. The energy and the radial reaction are given respectively by

$$E = -\chi f'(1) - y(f(1) - f(q_0)) - \beta f(q_{12}), \quad \mu = \chi f''(1) + (\chi + y)f'(1) - yq_0 f'(q_0) + \beta q_{12} f'(q_{12}). \quad (12)$$

The equations in (11) always admit the solution with $q_{12} = q_0 = 0$, representing the memoryless or ‘amnesic’ aging solution with parameters

$$\chi = \chi_{th} \equiv \frac{1}{\sqrt{f''(1)}}, \quad y = y_0 \equiv \frac{f''(1) - f'(1)}{f'(1)\sqrt{f''(1)}} = \frac{\sqrt{f''(1)}}{f'(1)} - \chi_{th}, \quad (13)$$

and consequently energy and radial reaction are given by

$$E = E_{th} \equiv -\chi_{th} f'(1) - y_0 f(1), \quad \mu = \mu_{th} \equiv 2\sqrt{f''(1)}. \quad (14)$$

For the (3+4)-spin model the numerical values are $\chi_{th} = 1/3$, $y_0 = 11/21 \simeq 0.52381$, $E_{th} = -71/42 \simeq -1.69048$ and $\mu_{th} = 6$.

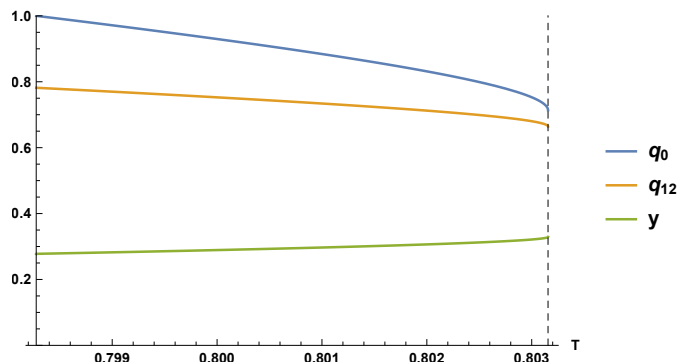


FIG. 9. Aging solution with memory of the initial configuration as predicted by the derivative of the Franz-Parisi potential for the (3+4)-spin model. q_0 (blue line), q_{12} (orange line) and y (green line) as a function of T . The temperature range in the plot is between $T_{\text{SF}} = 0.7982754$ and $T_0 = 0.8031557$ (marked by a dashed vertical line). Notice that in this solution we have $y \approx 0.3$ quite far from the value $y \approx 0.52$ that we observe in the numerical solution to the dynamical equations. Also notice that q_{12} and q_0 have finite values when the solution appears at T_0 .

A non trivial ‘memorious’ aging solution with strictly positive values for q_{12} and q_0 , disconnected from the amnesic aging solution, exists only for temperatures below T_0 . Moreover at an even lower temperature T_{SF} we have that $q_0 \rightarrow 1$ and this solution becomes replica symmetric. In Fig. 9 we report the values of q_0 , q_{12} and y in the memorious aging solution. In the (3+4)-spin model the existence domain for this solution is upper bounded by $T_0 = 0.8031557$ where the solution disappears by a square root singularity and lower bounded by $T_{\text{SF}} = 0.7982754$, where $q_0 \rightarrow 1$ and the solution becomes RS. At $T = T_{\text{SF}}$ the parameters extremizing the potential can be computed analytically. The value of q_{12} is more easily obtained from the RS solution (see below), while the value of y can be obtained from the third order expansion in $\varepsilon = 1 - q_0$ of the difference between the two equations in (11), thus getting

$$y(T_{\text{SF}}) = \frac{f'''(1)}{2[f''(1)]^{3/2}} \quad (15)$$

The numerical integration of dynamics does not give any indication in favour of this solution, in particular for the (3+4)-model, this solution has $y \approx 0.3$ in the whole range of validity, which is incompatible with the value $y \approx 0.52$ the

the numerics suggest. Even if we were disposed to believe that the dynamics would slowly cross-over to this solution on time scales we cannot observe numerically, still this would not solve the puzzle of the behavior of the asymptotic energy going below threshold for $T > T_{\text{MCT}}$. In this solution, the value of q_0 tends to 1 at temperature T_{SF} , well above the temperature of the static (Kauzmann) phase transition of the model. The one above is the only aging solution that we found, we searched, without finding, more complex solutions with more than one effective temperatures.

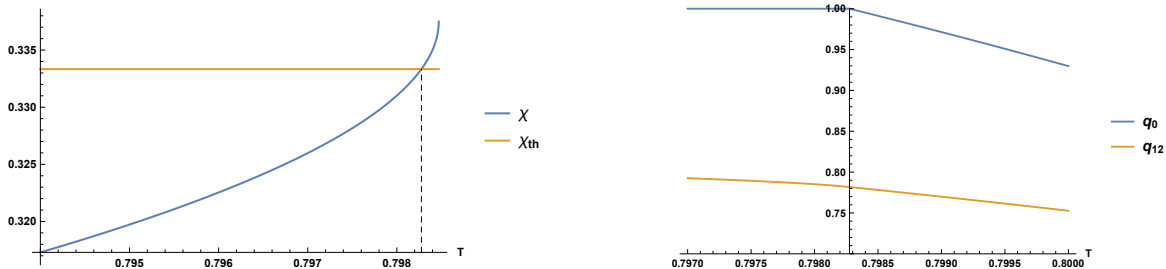


FIG. 10. Left: Susceptibility χ in the RS ‘state following’ solution for the (3+4)-spin model. $T_{\text{SF}} = 0.7982756$ is defined from the condition $\chi = \chi_{th}$, marked by a vertical dashed line. Right: Being the vertical axis located exactly at $T = T_{\text{SF}}$, values for q_0 and q_{12} on the right are from the RSB aging solution, while those on the left are from the RS ‘state following’ solution.

When $q_0 \rightarrow 1$ the 1RSB potential reduces to the RS potential

$$-2V_{\text{RS}}(q_{12}, \chi) = \chi f'(1) + \frac{1 - q_{12}^2}{\chi} + 2\beta f(q_{12}), \quad (16)$$

and saddle point equations read

$$\begin{cases} 1 - q_{12}^2 - \chi^2 f'(1) = 0 \\ q_{12} - \chi \beta f'(q_{12}) = 0 \end{cases} \quad (17)$$

with the energy taking the value $E = -\chi f'(1) - \beta f(q_{12})$. In the 3+4 model, the energy of this solution at T_{SF} is equal to $E_{\text{SF}} = -1.69981$ and decreases below. The susceptibility χ takes the marginal value χ_{th} at T_{SF} and becomes smaller than this value at lower T , as shown in the left panel of Fig. 10. Our estimate $T_{\text{SF}} = 0.7982756$ comes exactly from imposing $\chi = \chi_{th}$ in this RS solution. In the right panel of Fig. 10 we plot the value of q_0 and q_{12} obtained in the RS ‘state following’ solution on the left of the vertical axis, which is located exactly at $T = T_{\text{SF}}$. On the right of the vertical axis we report the corresponding values computed in the aging RSB solution (the same plotted in Fig. 9). We observe that q_{12} is a smooth function at T_{SF} . Its value right at T_{SF} can be computed analytically from the first equation in (17) by imposing $\chi = \chi_{th}$, leading to

$$q_{12, \text{SF}} = \sqrt{1 - \frac{f'(1)}{f''(1)}}. \quad (18)$$

For $T \leq T_{\text{SF}}$ the FP potential has a secondary minimum described by a replica symmetric ansatz. So we are effectively describing the quenching process from temperature T to zero temperature as a ‘state following’ process [10]: the observation that both at the starting and ending temperatures the state we are following is well described by a replica symmetric ansatz is an evidence that static-dynamics equivalence hold in this case. And this is what we indeed observe by comparing the asymptotic dynamics obtained integrating numerically the dynamical equations to the values derived here from the thermodynamic FP potential. For $T \leq T_{\text{SF}}$ aging disappears and one finds a simple agingless relaxation within a state described by the parameters computed in the secondary minimum of the FP potential.

III. SEMI-EMPIRICAL RELATIONS TO DESCRIBE THE LARGE TIMES DYNAMICS

We have seen that there is no simple aging solution to the asymptotic equations with $q_{12} > 0$ that is consistent with the finite time numerical integration of the dynamical equations. Nonetheless the FD plot in the mixed (3+4)-spin model do not differ in any appreciable way from the usual ones of the pure p -spin model with a single effective temperature and a value of y equal to the one that holds for the $\beta = 0$ initial condition. Insisting in representing the

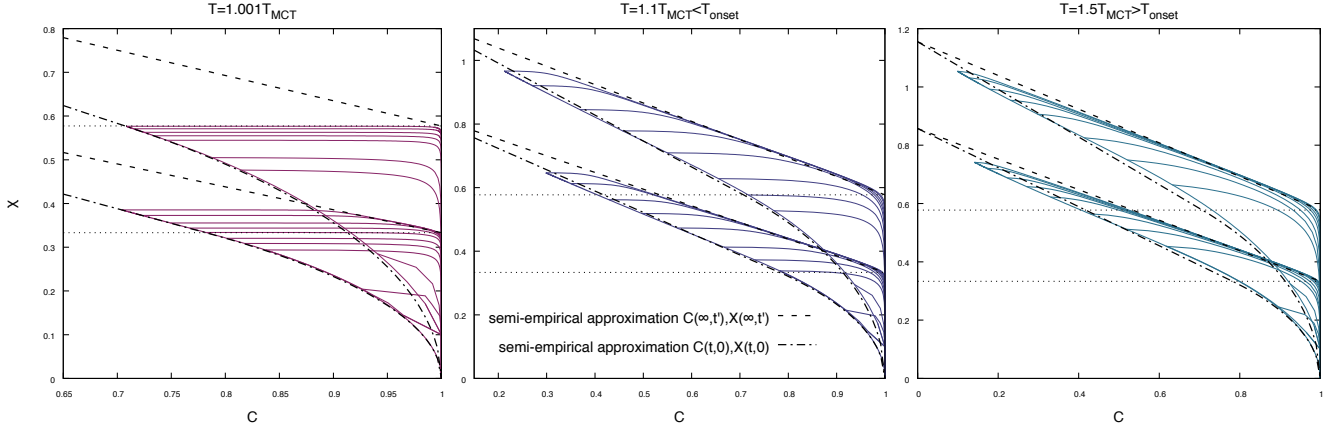


FIG. 11. FD curves $\chi(t, t')$ versus $C(t, t')$, each one with a different largest time t , plotted parametrically varying the smallest time t' . In each panel, upper data are for the pure 3-spin model, while lower data are for the mixed (3+4)-spin model. Notice that the 3 panels have different scales, but the dashed and dash-dotted curves are the same in all panels (see text for their definition).

best that we can the data in the *hic sunt leones* region with a single effective temperature dynamical ansatz, we ask what kind of relation can be derived between the overlaps q_0 and q_{12} . We suppose that μ, χ take the marginal values $\mu_{th} \equiv 2\sqrt{f''(1)}$ and $\chi_{th} \equiv 1/\sqrt{f''(1)}$. Moreover we assume the FD slope in the range $C(t, t') \in [q_0(t), 1]$ is independent of the initial temperature, thus it is equal to value obtained with $\beta = 0$, i.e. $y_0 \equiv \sqrt{f''(1)}/f'(1) - 1/\sqrt{f''(1)}$. Finally we assume the response is null in the range $C(t, t') \in [C(t, 0), q_0(t)]$, where the correlation decays extremely fast.

Within this 1RSB ansatz the asymptotic value for the radial reaction is given by

$$\mu = \chi f''(1) + (\chi + y)f'(1) - yf'(q_0)q_0 + \beta f'(q_{12})q_{12} \quad (19)$$

and by imposing $\mu = \mu_{th}$, $\chi = \chi_{th}$ and $y = y_0$ we get the relation

$$y_0 f'(q_0)q_0 = \beta f'(q_{12})q_{12} \quad (20)$$

that must hold on the asymptotic solution. We can notice at this point, that using (12) the energy can be written as $E = E_{th} + \Delta E$ with $\Delta E = yf(q_0) - \beta f(q_{12})$. Only in the pure model eq. (20) implies $\Delta E = 0$, in all the other cases it gives a non vanishing ΔE .

A second relation between q_0 and q_{12} can be derived from the observation of the FD plots in Fig. 11, where each curve is a parametric plot of $\chi(t, t')$ versus $C(t, t')$ at fixed t varying t' . We notice that, below the onset temperature, the points $(C(t, 0), \chi(t, 0))$ follows closely the dash-dotted curve that we are going to derive analytically. It is important to remark that the dash-dotted curve is the same in all the panels of Fig. 11, so it is a temperature independent relation. Also the dashed line is temperature independent and corresponds to the FD relation in the aging solution with $\beta = 0$, that is a line of slope $-y_0$ connecting the points $(0, \chi_{th} + y_0)$ and $(1, \chi_{th})$.

In order to obtain the dash-dotted line we assume that in the aging regime (i.e. for $\chi(t, 0) \geq \chi_{th}$) the relation between $C(t, 0)$ and $\chi(t, 0)$ is linear, while in the regime $\chi(t, 0) < \chi_{th}$ the dynamics is asymptotically exploring a state and thus we assume the relation that holds within the RS ‘state following’ solution. The latter can be easily derived from the first equation in (17)

$$\chi = \sqrt{\frac{1 - q_{12}^2}{f'(1)}} \quad (21)$$

that thus holds for $q_{12} \in [q_{12, SF}, 1]$, while the linear part has slope $-y_0/q_{12, SF}$ and passes through the points $(0, \chi_{th} + y_0)$ and $(q_{12, SF}, \chi_{th})$. We notice that the dash-dotted curve has a continuous first derivative at the point $(q_{12, SF}, \chi_{th})$, as can be easily checked by taking derivatives.

Our asymptotic ansatz thus implies a very simple relation between the overlaps describing the asymptotic aging regime, namely

$$q_{12} = q_{12, SF} q_0, \quad (22)$$

and plugging this relation inside Eq. (20) it is easily to find that a solution with $q_{12} > 0$ can exist only if

$$T < T_{\text{onset}} \equiv \frac{q_{12,\text{SF}}^k}{y_0} = \frac{f'(1)[f''(1) - f'(1)]^{\frac{k}{2}-1}}{f''(1)^{\frac{k-1}{2}}}, \quad (23)$$

where k is defined by $f(q) \propto q^k$ for $q \rightarrow 0$ (in the 3+4-model $T_{\text{onset}} = 0.91$). Despite this is not an exact solution of the asymptotic equations, it is a strong indication that there is a phase transition between a memoryless phase where dynamics decorrelate from the initial condition and falls over the ‘usual’ threshold states with $E = E_{th}$ and a phase where aging takes place in a confined space, with an asymptotic energy below threshold and depending on β .

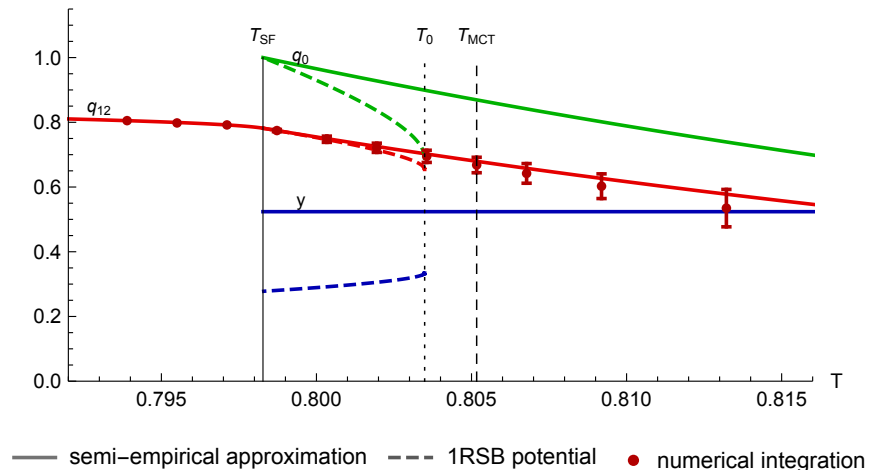


FIG. 12. Comparison between asymptotic aging parameters extrapolated from the numerical solution of the dynamical equations (data with errors), the analytical prediction obtained via the semi-empirical approximation derived in Sec. III (full curves) and the standard RSB aging solution derived in Sec. II (dashed curves).

In Fig. 12 we report an even stronger evidence that this approximate solution provides a very good description of the asymptotic dynamics obtained by numerically integrating the dynamical equations. We plot numerically extrapolated values as data points with errors, while full lines are prediction from the approximate solution presented in this Section and dashed lines correspond to the standard 1RSB aging solution discussed in the previous Section. Needless to comment on which one is better in describing the asymptotic dynamics.

IV. COUNTING THE MINIMA

In this section we ask then if we can understand the attractors of the dynamics in terms of typical marginal saddles and minima that lie close to the initial configuration. Let us consider the stationary points of the Hamiltonian $H[\sigma]$ on the sphere $\sum_i \sigma_i^2 = N$:

$$H'_i + \mu \sigma_i = 0. \quad (24)$$

As in dynamics, the radial reaction μ , takes, in any stationary point, the value

$$\mu = -\frac{1}{N} \sum_i \sigma_i H'_i. \quad (25)$$

We wish to classify the stationary points according to their energy $E = \frac{1}{N} H[\sigma]$ and the value of the radial reaction μ .

Differently from the pure models where $\mu = pE$, the relation between E and μ here is not univocal and stationary points are found in a whole region of the (E, μ) plane. Let us now consider the Hessian matrix $M_{ij} = H''_{ij} + \mu \delta_{ij}$ of the stationary points. It is well known [19] and rigorously proven [20] that H_{ij} is a GOE random matrix with variance $\text{Var}[H''_{ij}] = \frac{1}{N} f''(1)$. M has a semicircular spectral distribution with lower edge $\lambda_{min} = \mu - 2\sqrt{f''(1)} = \mu - \mu_{th}$. Stationary points are therefore minima if $\mu > \mu_{th}$ and saddles (or maxima) if $\mu < \mu_{th}$. As mentioned in the text, all marginal minima lie on the manifold $\mu = \mu_{th}$, which helps us to understand why in the dynamics the radial reaction always converges to that value in the aging regimes. Moreover, for any minimum we can compute the local

susceptibility $\chi(\mu) \equiv \frac{1}{N} \sum_i \left(\frac{\partial \sigma_i}{\partial h_i} \right) = \frac{1}{N} \text{Tr}(\mathbf{H}'' + \mu \mathbf{I})^{-1} = \frac{1}{2f''(1)} (\mu + \sqrt{\mu^2 - 4f''(1)})$, which in marginal minima take the value $\chi(\mu_{th}) = f''(1)^{-\frac{1}{2}} = \chi_{th}$ which is consistent with the jump of the integrated response in dynamics we observe in the numerical data. We conclude that for $T > T_{\text{SF}}$ dynamics is attracted by some family of marginal minima. In order to characterize these minima, we count the number of stationary points of the Hamiltonian $H[\boldsymbol{\sigma}]$ with fixed energy E and radial reaction μ that lie at a fixed overlap $\boldsymbol{\sigma} \cdot \boldsymbol{\sigma}_0 = Nq_{12}$ from a reference configuration $\boldsymbol{\sigma}_0$, weighted with a Gibbs measure $e^{-\beta H[\boldsymbol{\sigma}]}$. Since the complexity, i.e. the logarithm of their number, is self-averaging, we write

$$\Sigma(E, \mu, q_{12}, \beta) = \int_{S_N} \mathcal{D}\boldsymbol{\sigma}_0 \frac{e^{-\beta H[\boldsymbol{\sigma}_0]}}{Z_\beta} \log \left(\int_S \mathcal{D}\boldsymbol{\sigma} \delta(Nq_{12} - \boldsymbol{\sigma} \cdot \boldsymbol{\sigma}_0) \delta(NE - H) \delta(\mu\boldsymbol{\sigma} + \mathbf{H}') |\det(\mu\mathbf{I} + \mathbf{H}'')| \right) \quad (26)$$

The computation of Σ is standard, and can be performed in several steps. First of all, since the matrix \mathbf{H}'' is a GOE random matrix, the distribution of eigenvalues of $\mu\mathbf{I} + \mathbf{H}''$ is self-averaging and is a shifted semicircular $\rho(\lambda) = \frac{2}{\pi 4f''(1)} \sqrt{4f''(1) - (\lambda - \mu)^2}$. The modulus of the determinant $|\det(\mu\mathbf{I} + \mathbf{H}'')|$ is self-averaging and its logarithm reads

$$\begin{aligned} D(\mu) &= \frac{1}{N} \log |\det(\mu\mathbf{I} + \mathbf{H})| = \\ &= \text{Re} \left[\frac{1}{4f''(1)} (\mu^2 - \mu\sqrt{\mu^2 - 4f''(1)} - 2f''(1)) \left(-2 \log \left(\sqrt{\mu^2 - 4f''(1)} + \mu \right) + 1 + \log(4) \right) + \mu^2 \right] \quad (27) \end{aligned}$$

which only depends on μ . The imaginary part of this expression is the proportion of negative eigenvalues.

To evaluate the remaining terms we use replicas and write $\Sigma \equiv \overline{\log(\mathcal{N})} = \lim_{n \rightarrow 0} \frac{\overline{N^n - 1}}{n}$. We concentrate to the case of temperatures greater than the static transition temperature ($T > T_K$) of the model where the partition function appearing in the denominator of (26) is self-averaging and takes its annealed value $\overline{Z_\beta} = e^{\frac{N}{2}\beta^2 f(1)}$. One can then average over the disorder and the configuration $\boldsymbol{\sigma}_0$ at the same time. Opening the delta function in the Fourier basis,

$$\Sigma(E, \mu, p, \beta) = \lim_{n \rightarrow 0} \frac{1}{n} \left(e^{-\frac{1}{2}\beta^2 f(1)} \int \mathcal{D}_S e^{\sum_a N(i\hat{\beta}_a E - i\hat{\sigma}_a \cdot \boldsymbol{\sigma}_a \mu)} \delta(Nq_{12} - \boldsymbol{\sigma}_a \cdot \boldsymbol{\sigma}_0) \overline{e^{-\beta H_0} e^{\sum_a^n (i\hat{\beta}_a + i\hat{\sigma}_a \cdot \nabla) H_a}} \right) + ND(\mu) \quad (28)$$

where $\int \mathcal{D}_S = \int_S \mathcal{D}\boldsymbol{\sigma}_0 \prod_a \left(\int_S \mathcal{D}\boldsymbol{\sigma}_a \int \mathcal{D}\hat{\sigma}_a \int \hat{\beta}_a \right)$.

And since the disorder is Gaussian :

$$\overline{e^{-\beta H_0} e^{\sum_a^n (i\hat{\beta}_a + i\hat{\sigma}_a \cdot \nabla) H_a}} = e^{\frac{1}{2} \left(\beta^2 f \left(\frac{\boldsymbol{\sigma}_0 \cdot \boldsymbol{\sigma}_0}{N} \right) + 2\beta \sum_a (i\hat{\beta}_a + i\hat{\sigma}_a \cdot \nabla) f \left(\frac{\boldsymbol{\sigma}_a \cdot \boldsymbol{\sigma}_0}{N} \right) + \sum_{ab} (i\hat{\beta}_a + i\hat{\sigma}_a \cdot \nabla^a) (i\hat{\beta}_b + i\hat{\sigma}_b \cdot \nabla^b) f \left(\frac{\boldsymbol{\sigma}_a \cdot \boldsymbol{\sigma}_b}{N} \right) \right) \Big|_{\boldsymbol{\sigma} \rightarrow \boldsymbol{\sigma}_0}}$$

Now we define overlap variables $NQ_{ab} = \boldsymbol{\sigma}_a \cdot \boldsymbol{\sigma}_b$, $N\chi_{ab} = i\boldsymbol{\sigma}_a \cdot \hat{\boldsymbol{\sigma}}_b$ and $NR_{ab} = -\hat{\boldsymbol{\sigma}}_a \cdot \hat{\boldsymbol{\sigma}}_b$, and the overlaps with the reference configuration $Nq_{12} = \boldsymbol{\sigma}_a \cdot \boldsymbol{\sigma}_0$, $N\chi_p = i\hat{\boldsymbol{\sigma}}_a \cdot \boldsymbol{\sigma}_0$. This change of variables defines a matrix:

$$\mathcal{Q} \equiv \begin{pmatrix} 1 & q_{12} & -i\chi_p \\ q_{12} & Q_{ab} & -i\chi_{ab} \\ -i\chi_p & -i\chi_{ab} & -R_{ab} \end{pmatrix}$$

where $Q_{aa} = 1$ due to the spherical constraint. And, from the equivalence between replicas, we fix $i\hat{\beta}_a = y$ and $\chi_{aa} = \chi \forall a$. With this change of variables Eq. (28) becomes

$$\begin{aligned} \Sigma &= (yE - \mu\chi) + \beta (yf(q_{12}) + \chi_p f'(q_{12})) + \lim_{n \rightarrow 0} \frac{1}{n} \left(\frac{1}{2} \log(\det \mathcal{Q}) \right) + D(\mu) \\ &+ \lim_{n \rightarrow 0} \frac{1}{n} \left(\frac{1}{2} \sum_{ab} [y^2 f(Q_{ab}) + 2yf'(Q_{ab})\chi_{ab} + f'(Q_{ab})R_{ab} + f''(Q_{ab})(\chi_{ab})^2] \right) \quad (29) \end{aligned}$$

where $\frac{1}{2} \log(\det \mathcal{Q})$ is the volume factor that comes from the change of variables from spins to overlaps. To get the leading N contribution we must extremize with respect to all the overlap parameters \mathcal{Q} and y . We notice that a further simplification to the expression (29) can be obtained by firstly extremizing with respect to R_{ab} . Assuming a replica symmetric ansatz for the overlap matrices Q and χ , i.e. $Q = \delta_{ab} + (1 - \delta_{ab})q_0$ and $\chi_{ab} = \delta_{ab}\chi + (1 - \delta_{ab})\chi_1$ we get, in the limit $n \rightarrow 0$:

$$\begin{aligned} \Sigma(E, \mu, q_{12}, \beta; y, \chi, \chi_1, \chi_p, q_0) &= +yE - \mu\chi + \beta[yf(q_{12}) + \chi_p f'(q_{12})] \\ &+ \frac{1}{2} [y^2 (f(1) - f(q_0)) + 2y(f'(1)\chi + f'(q_0)\chi_1) + \mathcal{R} + (\chi^2 f''(1) - \chi_1^2 f''(q_0))] \quad (30) \\ &+ \frac{1}{2} (\log(1 - q_0) + \frac{q_0 - q_{12}^2}{1 - q_0} - \log(f'(1) - f'(q_0)) - \frac{f'(q_0)}{f'(1) - f'(q_0)}) + D(\mu) \end{aligned}$$

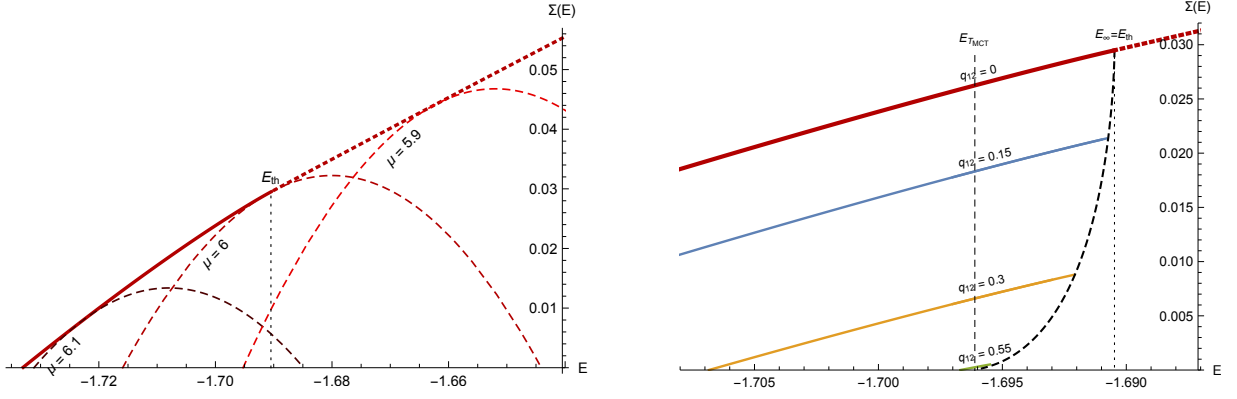


FIG. 13. Left: Complexity $\Sigma(E)$ of the (3+4)-spin model as a function of the energy E . The full red line represents the complexity of the dominant stable minima. Its continuation above E_{th} represents the complexity of the dominant saddles. The dashed lines represent the complexity fixing the radial reaction: $\mu = \mu_{th} = 6$ corresponds to marginal minima, $\mu > 6$ to stable minima and $\mu < 6$ to saddles. Right: Complexity constraining the system at a fixed overlap q_{12} from a reference configuration sampled at temperature $T = T_{MCT}$. Vertical lines mark energy values E_{∞} and $E_{T_{MCT}}$ corresponding to extrapolated asymptotic energies reached by the dynamics starting respectively from $T = \infty$ and $T = T_{MCT}$. The dynamics starting from a random configuration goes to the *most numerous marginal minima* ($E_{\infty} = E_{th}$), while starting near T_{MCT} the dynamics goes below E_{th} . Constraining to an overlap $q_{12} > 0$ from the initial configuration provides a qualitatively correct explanation: the energy of the most numerous marginal minima decreases.

where

$$\mathcal{R} \equiv 1 + f'(1) \left(\frac{\chi - \chi_1}{1 - q_0} \left((\chi - \chi_1) - \frac{q_0 - q_{12}^2}{1 - q_0} + 2(\chi_1 - p\chi_p) \right) + \chi_p^2 \right) - f'(q_0) \left(\frac{\chi - \chi_1}{1 - q_0} \left(-\frac{q_0 - q_{12}^2}{1 - q_0} + 2(\chi_1 - p\chi_p) \right) + \chi_p^2 \right) \quad (31)$$

This can be extremized explicitly with respect to y, χ, χ_1, χ_p , while q_0 -extremization has to be done numerically. For $q_{12} = 0$ the solution is $q_0 = 0$ and we recover the expression found in [22]

$$\Sigma(E, \mu) = \max \left\{ 0, \text{Re} \left(-\frac{(E^2 (f''(1) + f'(1)) + 2E\mu f'(1) + f(1)\mu^2)}{2f(1)(f''(1) + f'(1)) - f'(1)^2} \right. \right. \\ \left. \left. + \frac{\mu}{\sqrt{\mu^2 - 4f''(1)} + \mu} + \log \left(\sqrt{\mu^2 - 4f''(1)} + \mu \right) + \frac{1}{2} \log \left(\frac{1}{f'(1)} \right) - \log(2) \right) \right\} \quad (32)$$

In the left panel of Fig. 13 we see that, for any value of μ , Σ has a concave parabolic shape as a function of the energy and many values of the energy are possible for the same μ . In particular this is true for $\mu = \mu_{th}$: there is not a unique threshold energy (at variance to pure p -spin models), but a whole interval for which $\Sigma(E, \mu_{th}) > 0$. We define the dominating stationary points at a given value of the energy as the ones that maximize Σ as a function of μ . The threshold energy as defined from dynamics, corresponds to the values of the energy that separates minima from saddles on the dominating line. Notice that this value does not correspond to the most numerous marginal minima, which occurs for $\mu = \mu_{th}$ and $E > E_{th}$, but to the point where the most numerous stationary saddles become minima. This observation sheds some light on the dynamics from a white initial condition; minima are not accessible at levels of the energy $E > E_{th}$ where saddles dominate the landscape.

Extending the concept of threshold energy to the case $q_{12} > 0$ is straightforward. As shown in the right panel of Fig. 13 for any fixed value of q_{12} we can plot the curve corresponding to dominating minima. This curve ends at an energy value that we call $E_{th}(q_{12})$ and this is the best candidate for the asymptotic energy in the dynamics. Indeed for $E > E_{th}(q_{12})$ dominating stationary points are saddle and the dynamics is likely to keep relaxing to $E_{th}(q_{12})$.

In Fig. 14 we plot the quenched constrained complexity of marginal states in the (3+4)-spin model, computed with $T = T_{MCT}$ (left panel) and $T = 1.02 T_{MCT}$ (right panel). Please notice that the choice of the temperature is not crucial: as long as $T \in (T_{SF}, T_{onset})$ the plot would be very similar. The red curve in the plot represents the threshold energy $E_{th}(q_{12})$ defined above. We notice that the range of energies with a positive complexity is very large compared to variations in E_{th} . The green ellipses represents our best estimate for the large time limit of the actual dynamics solved numerically: while the energy can be very well estimated, the limit of $C(t, 0)$ is plagued by a large uncertainty due to its slow convergence (until now we have not attempted such an extrapolation, but here we want to be more speculative and we take the risk). From the plot one is tempted to conjecture that the dynamics always converges to marginal states with a threshold energy $E_{th}(q_{12})$. However, we have not found any principle to fix the value of q_{12}

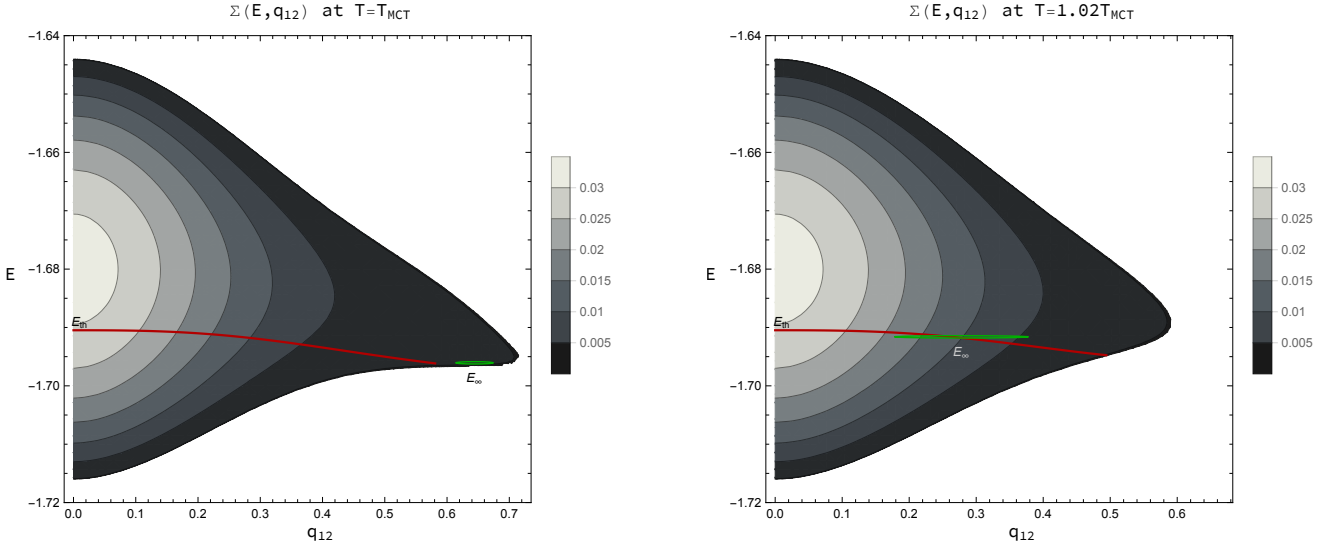


FIG. 14. The quenched complexity of marginal states ($\mu = \mu_{th}$) with energy E and overlap q_{12} with respect to an equilibrium configuration at temperature $T = T_{MCT}$ (left panel) and $T = 1.02 T_{MCT}$ (right panel). The choice of the temperature is not crucial as long as $T \in (T_{SF}, T_{onset})$. The red curve marks the threshold energy $E_{th}(q_{12})$ and the green ellipses is our best estimate for the the large time limit of the actual dynamics obtained from the numerical integration.

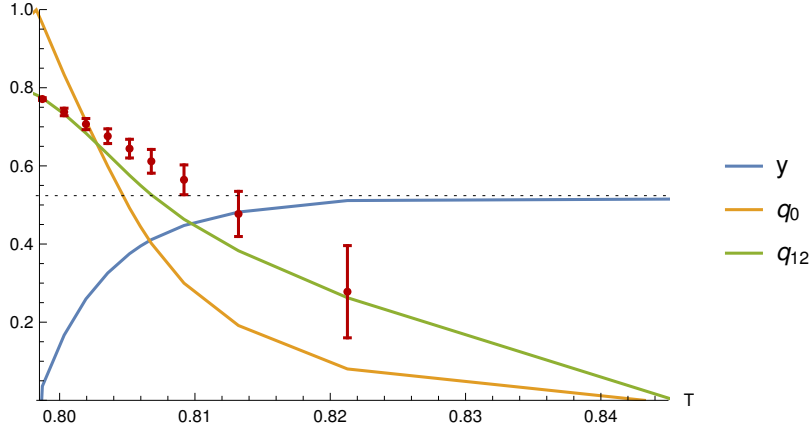


FIG. 15. Assuming the dynamics relaxes on the marginal manifold with energy $E_{th}(q_{12})$ and fixing the energy from the large time extrapolation of the numerical data, which in turn fixes the value for q_{12} , we can compute analytical values for the remaining aging parameters, namely q_0 and $y = \partial_E \Sigma$. While the estimate of q_{12} is compatible with the large time extrapolation of $C(t, 0)$ (red points with error in the figure), the other aging parameters are far from those measured in the actual dynamics.

solely from the complexity curve and further studies are needed to better match the large time limit of the dynamics to the energy landscape.

Although Fig. 14 may suggest that the constrained complexity is somehow predicting about the large time aging dynamics of mixed spherical models, a more careful analysis reveals its limitations. Assuming that at large times the relaxation dynamics converges to the manifold of marginal states belonging to the curve $E_{th}(q_{12})$ one could estimate the point reached by the dynamics by extrapolating the asymptotic energy $E_\infty(T)$ and estimating q_{12} from the equality $E_{th}(q_{12}) = E_\infty$. Having thus fixed the values of E and q_{12} one can proceed estimating the remaining parameters of the asymptotic aging dynamics, q_0 and $y = \partial_E \Sigma$, from the saddle point equations used to compute the quenched complexity. The result of this computation is shown in Fig. 15 with full lines, and compared to the (very uncertain) extrapolation of $C(\infty, 0)$, shown by red points with errors. We clearly see that, while the estimate of q_{12} is compatible with the actual dynamics, the other two parameters are far from the values measured in the numerical solution to the dynamics. Indeed q_0 becomes smaller than q_{12} while in the actual dynamics the inequality $q_{12} < q_0$ is always satisfied, and y becomes much smaller than y_0 (marked by a dotted horizontal line in Fig. 15) which is good descriptor of the actual aging in the whole temperature range studied. So, we believe the present computation

of the quenched complexity of marginal minima of the energy function in mixed p -spin models is not the end of the story, but only a quantitative way of understanding the limitation of the approach used up to now. Much more work will be required to connect the large time aging dynamics to the properties of the energy landscape (e.g. basins of attractions are likely to play an important role, but are at present absent in the computation).

-
- [1] S. Sastry, P. G. Debenedetti, and F. H. Stillinger, *Nature* **393**, 554 (1998).
 - [2] F. Sciortino, W. Kob, and P. Tartaglia, *Physical Review Letters* **83**, 3214 (1999), arXiv: cond-mat/9906081.
 - [3] A. Crisanti and H.-J. Sommers, *Zeitschrift fr Physik B Condensed Matter* **87**, 341 (1992).
 - [4] A. Crisanti, H. Horner, and H.-J. Sommers, *Zeitschrift fr Physik B Condensed Matter* **92**, 257 (1993).
 - [5] L. F. Cugliandolo and J. Kurchan, *Physical Review Letters* **71**, 173 (1993), arXiv: cond-mat/9303036.
 - [6] B. Kim and A. Latz, *Europhysics Letters (EPL)* **53**, 660 (2001), arXiv: cond-mat/0005172.
 - [7] J. Kurchan, G. Parisi, and M. Virasoro, *Journal de Physique I* **3**, 1819 (1993).
 - [8] S. Franz and G. Parisi, *Journal de Physique I* **5**, 1401 (1995), arXiv: cond-mat/9503167.
 - [9] A. Barrat, S. Franz, and G. Parisi, *Journal of Physics A: Mathematical and General* **30**, 5593 (1997), arXiv: cond-mat/9703091.
 - [10] Y. Sun, A. Crisanti, F. Krzakala, L. Leuzzi, and L. Zdeborová, *Journal of Statistical Mechanics: Theory and Experiment* **2012**, P07002 (2012), arXiv: 1204.3734.
 - [11] H. Sompolinsky and A. Zippelius, *Physical Review B* **25**, 6860 (1982).
 - [12] M. Mezard, G. Parisi, and M. Virasoro, *Spin Glass Theory and Beyond: An Introduction to the Replica Method and Its Applications*, World Scientific Lecture Notes in Physics (World Scientific, 1987).
 - [13] A. Barrat, R. Burioni, and M. Mzard, *Journal of Physics A: Mathematical and General* **29**, L81 (1996), arXiv: cond-mat/9511089.
 - [14] S. Franz and M. Mezard, *Physica A: Statistical Mechanics and its Applications* **210**, 48 (1994), arXiv: cond-mat/9403004.
 - [15] L. Berthier, G. Biroli, J.-P. Bouchaud, W. Kob, K. Miyazaki, and D. Reichman, *The Journal of Chemical Physics* **126**, 184504 (2007), arXiv: cond-mat/0609658.
 - [16] A. Crisanti and H.-J. Sommers, *Journal de Physique I* **5**, 805 (1995).
 - [17] L. F. Cugliandolo, J. Kurchan, and L. Peliti, *Physical Review E* **55**, 3898 (1997), arXiv: cond-mat/9611044.
 - [18] Relative variations of χ and y comparable to the one we find in the energy cannot be excluded.
 - [19] A. Cavagna, I. Giardina, and G. Parisi, *Physical Review B* **57**, 11251 (1998), arXiv: cond-mat/9710272.
 - [20] A. Auffinger, G. B. Arous, and J. Cerny, arXiv:1003.1129 [math-ph] (2010), arXiv: 1003.1129.
 - [21] B. Capone, T. Castellani, I. Giardina, and F. Ricci-Tersenghi, *Physical Review B* **74** (2006), 10.1103/PhysRevB.74.144301, arXiv: cond-mat/0603759.
 - [22] G. B. Arous, E. Subag, and O. Zeitouni, arXiv:1804.10573 [math] (2018), arXiv: 1804.10573.